Magnetoelectric micromachines with wirelessly controlled navigation and functionality

Originally published in:
Materials Horizons 3(2), https://doi.org/10.1039/c5mh00259a

Journal Name

COMMUNICATION

Magnetoelectric Micromachines with Wirelessly Controlled Navigation and Functionality

Received 00th January 20xx,
Accepted 00th January 20xx

DOI:

/

Xiang-Zhong Chen,[a] Naveen Shamsudhin,[a] Marcus Hoop,[a] Roel Pieters,[a] Erdem Siringil,[a] Mahmut Selman Sakar,[a] Bradley J. Nelson,[a] and Salvador Pané* [a]

The use of a single energy source for both manipulating micromachines and triggering their functionalities will result in highly integrated devices and simplify the design of the controlling platform. Here, we demonstrate this concept employing magnetoelectric Janus particle-based micromachines, which are fabricated by coating SiO_2 microspheres with a $CoFe_2O_4$-$BaTiO_3$ bilayer composite. While the inner magnetic $CoFe_2O_4$ layer enables the micromachines to be maneuvered using low magnitude rotating magnetic fields, the magnetoelectric bilayer composite provides the ability to remotely generate electric charges upon the application of a time-varying magnetic field. To demonstrate the capabilities of these micromachines, noble metals such as Au, Ag and Pt are magnetoelectrochemically reduced from their corresponding precursor salts and form nanoparticles on the surface of the micromachines. Magnetoelectric micromachines are promising devices for their use as metal scavengers, cell stimulators or electric field-assisted drug delivery agents.

Synthetic micro- and nanomachines hold great promise for their wide range of applications in biomedicine,[1-4] environmental remediation,[5-7] or microassembly.[8-10] In the last decade, research on small-scale machines has mainly focused on developing actuation methods for low-Reynolds number locomotion. Micro- and nanomachines can be propelled by providing either electromagnetic or mechanical energy (e.g. ultrasound) from an external power source[11-17] or by means of a chemical reaction occurring at the interface of the device and the liquid environment.[18-20] These studies have not only provided a better understanding of motion at micro- and nanoscale, but also supported the progress of cutting-edge fabrication methods and materials development.

[a] *Multi-Scale Robotics Lab (MSRL), Institute of Robotics & Intelligent Systems (IRIS), ETH Zurich, Zurich 8092, Switzerland. E-mail: vidalp@ethz.ch*

Electronic Supplementary Information (ESI) available: Experimental details, discussion on piezoelectrochemical reactions, XRD patterns of the bilayer composites, control experiment results on the plane thin films, PFM study of $BaTiO_3$ layer and magnetic loop of M-E Janus microspheres. See DOI:

Today, micromachines can be precisely navigated and positioned at target locations using magnetic fields.[3, 10, 21] Magnetic manipulation has several advantages over other methods of power delivery. Magnetic fields are biocompatible and can penetrate deep into non-transparent materials such as biological tissues.[1] Moreover, there are several approaches for maneuvering magnetic micromachines based on their shape, magnetic anisotropy and the applied control signal (oscillating fields, rotating fields or field gradients).[22-24] Once the micromachine reaches the region of interest, it must be triggered to interact with the local environment or to operate on a target material. Micromachines can be engineered using stimuli-responsive materials for passive triggering in response to local changes in pH or temperature.[3, 25, 26] However, such

Conceptual Insights

Micro- and nanorobots have attracted wide attention due to their great potential in various fields such as targeted delivery, minimally invasive surgery, and environmental remediation. Compared to microorganisms, which can be considered as highly integrated micromachines utilizing a single energy input (i.e., food) to effectively accomplish various missions (such as sensing, locomotion, reproduction, etc.), micro- and nanorobots are usually task-specific, and their integration level is still low. A typical drawback is that the power sources for controlled locomotion and on-demand function are different, which hinders the realization of highly-integrated multifunctional small scale micromachines together with simple manipulation systems. In this work, by integrating magnetoelectric materials, we take the first step to develop a prototype, which can be powered by a single energy source (magnetic energy) for both locomotion and on-demand function triggering, to enlighten the concept of highly-integrated micromachines with a simplified manipulation system. This concept not only presents a further step in the development of micromachines but also opens new avenues for the application of magnetoelectric materials. Magnetoelectric micromachines endowed with the ability to induce electrochemical reactions have the potential to find applications in targeted cell stimulation and environmental remediation.

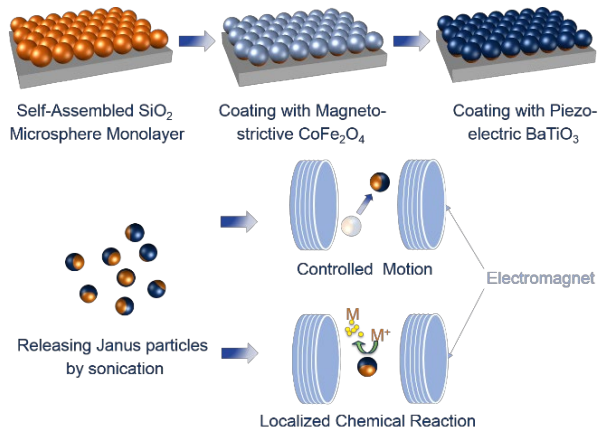

Scheme 1 Schematic illustration of fabrication process of magneto-electric Janus microparticles and their manipulation as well as applications for noble metal reduction reaction.

passive methods are only effective when there is a significant change in the target microenvironment, and this change must be specific to that location. As an alternative strategy, micromachines can be triggered on-demand using non-invasive external magnetic fields or light stimulation.[3, 7, 8] Utilizing a single energy source for both navigating the micromachine and triggering its functions will result in highly integrated devices and will simplify the design of the controlling platform.

Electromagnetic fields play an important role in many chemical and biological phenomena. The application of electric fields generally requires the presence of electrodes, which makes the whole process invasive. However, with the right choice of materials, electric fields can be wirelessly generated on untethered devices using external magnetic fields. Here we introduce magnetoelectric (ME) micromachines based on Janus microparticles that can be both maneuvered and triggered to generate electrical signals using external magnetic fields. ME materials can convert magnetic energy into electric output and have been utilized to build devices such as memories or sensors.[27, 28] Janus microparticles (JMPs) consist of two hemispheres of dissimilar materials and surface chemistry, and they find a variety of application areas due to the ease of fabrication and wide range of materials selection for functionalization.[29-31] They have been already employed as fuel-driven micromotors[32, 33] or magnetic microagents.[22, 34, 35] In this work, we explore the possibility of using JMPs as mobile micromachines navigated with uniform rotating low magnitude magnetic fields, and we demonstrate their ability of inducing localized electrochemical reactions at their surface upon application of time-varying high magnetic fields. Specifically, we show that generated surface charges on JMPs immersed in electrolytes can induce the reduction of noble metal ions. Implementation of ME building blocks in micro- and nanomachines will provide novel functionalities in environmental and biomedical applications including metal recovery, cell electrostimulation or electrically-assisted drug delivery.

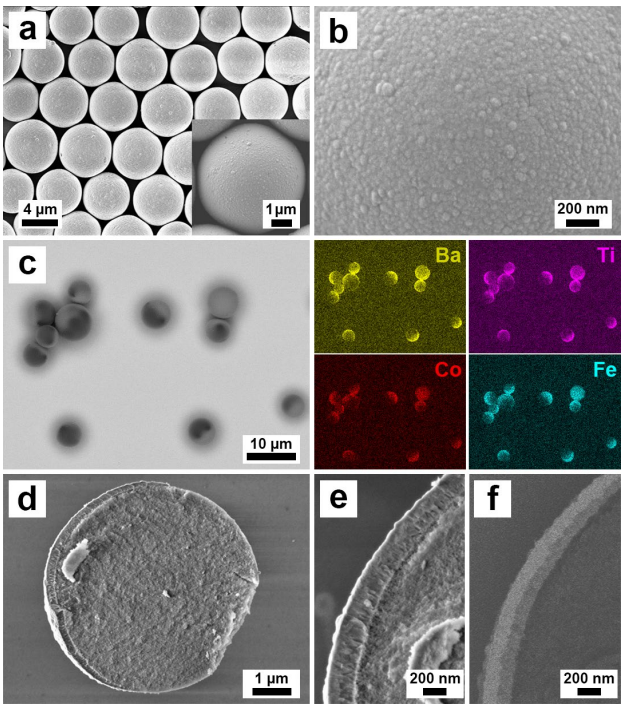

Figure 1 (a) An SEM image showing self-assembled monolayer of silica spheres coated with $CoFe_2O_4$ and $BaTiO_3$. The inset shows a magnified image of a single microsphere. (b) A magnified SEM image showing the details of the $BaTiO_3$ coating. (c) A BSE-SEM image (left panel) and the corresponding EDX element distribution mapping (right panels) of a few released Janus particles. (d) An SEM image of a broken JMP showing the cross-section of the ME coating. The details of the coating are magnified and shown using SE (e) and BSE (f) SEM images.

The fabrication protocol of ME JMPs is illustrated in Scheme 1. First, a self-assembled monolayer of silica microspheres (~ 5 µm) was prepared on a piece of silicon chip by means of dip-coating. The chip was then coated with a magnetostrictive $CoFe_2O_4$ layer and a piezoelectric $BaTiO_3$ layer by magnetron sputtering at 600 °C. Under a programmed magnetic field, the magnetostrictive layer deforms, and the generated strain is transferred to the piezoelectric layer through interfacial coupling, which in turn becomes electrically polarized. The charges on the surface are used for inducing electrochemical reactions. The magnetic material is only deposited on one hemisphere, JMPs exhibit magnetic shape anisotropy, which enables rolling motion under low magnitude rotating magnetic fields.

Figure 1 shows a self-assembled monolayer of silica spheres after sputtering with $CoFe_2O_4$ and $BaTiO_3$. The spheres exhibit a hexagonal close packing arrangement when they have similar size. The densely packed particles remain intact even after high temperature treatment, showing good compatibility with the sputtering process. The inset shows a magnified image of a single particle in which it can be observed that the surface facing the sputtering sources is uniformly coated. The granular surface suggests a polycrystalline coating, which is further confirmed by means of X-ray diffraction (Figure S1). An investigation of the surface morphology in Figure 1(b) shows that the size of the crystalline

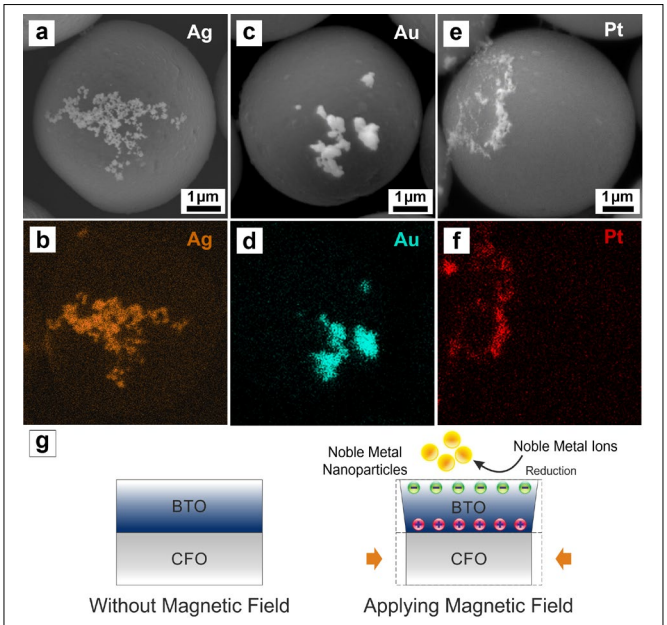

Figure 2 SEM images (a, c, e) of ME Janus microsphere with noble metal nanoparticles on top after reduction experiments. The corresponding element distribution EDX maps (b, d, f) confirm the composition of the nanoparticles. (g) Schematic illustration of procedures for magneto-electro-chemical reduction of noble metal ions.

grains varies from tens of to more than a hundred nanometers. Figure 1(c) displays a back-scattered electron (BSE) image obtained by scanning electronic microscopy (SEM), from which elements with large differences in atomic number can be distinguished. The elements in the coatings (Ba, Ti, Co, Fe) have higher atomic numbers than Si. Therefore, these elements display a brighter contrast in the image due to a stronger scattering of electrons by their larger atomic nuclei. The differences in contrast between the two hemispheres of the microparticles clearly show the characteristic double face of a JMP. The elementary distribution is confirmed by energy dispersive X-ray analysis (EDX) mapping of the same area. The Ba-, Ti- (from $BaTiO_3$) and Co-, Fe- (from $CoFe_2O_4$) rich zones observed in the EDX maps correspond well to the brighter parts in the BSE-SEM images. However, one can notice a decrease of color intensity within the coated hemisphere toward the uncoated part, which indicates a gradual change in the amount of sputtered material. This is also corroborated by the cross-sectional SEM image shown in Figure 1(d). The thickness of the coating is the largest in the middle of the sphere, and it becomes smaller towards the edge. This is caused by the shadowing effect of adjacent spheres, because the sputtering gun is tilted 35 degrees with respect to the substrate surface normal. An investigation of the ME coating reveals a conformally coated bilayer thin film on the sphere (Figure 1(e) and (f)). The thin film bilayer is approximately 250 nm in thickness, each layer being around 125-nm thick. A clear interface is observed between the two layers and no voids are observed. For an efficient coupling between the two layers, a high-quality interface is desired since the interface plays an important role in mediating the response from the magnetostrictive layer to the piezoelectric layer, realizing the ME coupling.[27, 36, 37]

The reduction of noble metal ions via the ME effect was carried out by positioning the JMPs in the metal salt solutions under a large DC magnetic field (800 Oe) superimposed with a small AC field (50 Oe) at room temperature. The results are shown in Figure 2. It can be seen that silver, gold, and platinum can be deposited as nanoparticles adsorbed onto the microspheres, respectively. The EDX mapping shows that the elementary distribution corresponds well with the morphology observed in the SEM images. It is important to note that the photochemical properties of ferroelectric $BaTiO_3$ surface have been previously reported.[38-41] To exclude the influence of possible photochemical effects, the ME experiments were all conducted in darkness. Several control experiments were also designed (Experimental section in Supporting Information and Figure S2). In the absence of magnetic fields, no particles were found on ME bilayer chips. Formation of nanoparticles was also not observed on chips with only a $BaTiO_3$ layer or a $CoFe_2O_4$ layer when the JMPs were subject to magnetic fields. The control experiments indicate that nanoparticles are formed due to a magnetoelectrically induced chemical reaction. However, the mechanism for the magnetoelectrochemical process remains unclear, although the ME effect has already been employed to induce certain chemical processes, as reported elsewhere.[42-45] For example, Khizroev and co-workers demonstrate an on-demand release of an anti-human immunodeficiency virus drug from $CoFe_2O_4$@$BaTiO_3$ core-shell ME nanocarriers. The drug-carrier bond can be broken by applying a low alternating magnetic field due to the induced ME effect.[44] In this case, the repulsion caused by the polarization on the carrier surface leads to the cleavage of the drug-carrier bond. In our case, a pathway can occur when a magnetic field is applied, and the $CoFe_2O_4$ layer experiences a strain. Due to interfacial coupling, the strain will be transferred to the piezoelectric $BaTiO_3$ layer, and thus its polarization state will be changed. This causes a potential difference across the piezoelectric surface / electrolyte interface.[46] When the grain size is smaller than several tens of nanometers, the energy barrier for generating charge carriers in $BaTiO_3$ becomes much smaller (one magnitude lower than the coarse-grain counterpart).[47] As a result, the electron-hole pairs are easily generated from the strained $BaTiO_3$,[48] and the potential difference becomes a driving force for the electron transfer across the solid/solution interface.[46] Finally, electrochemical reactions such as the reduction of metal ions near the surface is induced. It should also be noted that the electrical potential induced by strains less than 10 ppm in $BaTiO_3$ is already enough to induce the water-splitting reaction.[49, 50] As the maximum magnetostriction generated by $CoFe_2O_4$ is -590 ppm along its <100> direction, it is expected that strains on the order of tens of ppm will occur in the piezoelectric layer.[51] In addition, all the electrochemical potentials for the reduction of silver, gold and platinum ions are more positive than that of the hydrogen reduction (Table 1), which means that the metal deposition can be feasibly induced at even lower strain levels.

Table 1 Standard reduction potentials

Reduction half reaction	E^0 (V)
$2H^+$ (a.q.) + $2e^- \rightarrow H_2$ (g)	0
Ag^+ (a.q.) + $e^- \rightarrow$ Ag (s)	0.7991
$AuCl_4^-$ (a.q.) + $3e^- \rightarrow$ Au(s) + $4Cl^-$ (a.q.)	1.002
$PtCl_6^{2-}$ (a.q.) + $4e^- \rightarrow$ Pt (s) + $6Cl^-$ (a.q.)	0.726

The metals are deposited in the form of agglomerated nanoparticles instead of a uniform thin film on the JMPs. There are several possible reasons for this phenomenon. First, magnetoelectrochemical active sites are randomly distributed due to the polycrystalline nature of the thin films. One must take into account that the magnetostriction of $CoFe_2O_4$ differs along different crystalline axes. Therefore, the magnetostrictive properties on different crystalline grains vary significantly in terms of both magnitude and direction. Similarly, the piezoelectric properties in $BaTiO_3$ layers also vary from grain to grain due to random crystal orientation. Second, there is a detrimental effect when reducing the size of ferroelectric grains, which results in a mixture of piezoelectric tetragonal and non-piezoelectric cubic phases in $BaTiO_3$ films.[52] These size effects tend to increase the non-uniform distribution of piezoelectric properties. This can be confirmed by our PFM measurements (Figure S3) as well as by the results reported in other work.[53] The non-uniform distribution of both magnetostrictive and piezoelectric domains results in a random distribution of ME active sites. Third, differences in the ME layer thickness on the microsphere also contribute to the non-uniform distribution of ME active sites. Therefore, deposition of uniform thin metal films is not observed. Instead, nanoparticles are formed from the reduction of noble metal salts. Nanoparticles might form either directly on the surface of the ME layers, or near their surface and then adsorb onto it. Judging from the observed nanoparticle aggregation, a combination of both routes seems plausible. In addition, the clamping effect between the substrate (herein the SiO_2 microsphere) and the composite layer tends to reduce the magnetoelectric effect, which also contributes to the low efficiency of the reduction reaction. Unfortunately, it is difficult to quantify the reaction efficiency of this system due to the random distribution of ME active sites, because some particles can be washed away during the cleaning step.

To fulfill specific tasks at a certain location, targeted movement of the ME JMPs is necessary. Most reports on mobile Janus particles rely on the catalyzed decomposition of chemical fuels such as H_2O_2 or N_2H_4.[20] However, under conditions where chemical fuels are not available, their applications are highly restricted.[54] The orientation and position of JMPs can be magnetically controlled due to the $CoFe_2O_4$ layer deposited on the particles. Vibrating sample magnetometry (VSM) analysis showed that the coercive fields of the particles are close to 1500 Oe (Figure S4). Therefore, for field strength values significantly lower than 1500 Oe, the microsphere will not exhibit a change in its magnetization but will experience a torque and align along the field lines. Figure 3 demonstrates the remote control of JMPs using a uniform magnetic field of 100 Oe. The cap follows the direction of the magnetic field rotating around the z-axis as shown in Figure 3(a) (see also Movie S1, Supporting Information). The particles aligned without translation during these manipulation experiments, indicating that magnetic field gradients were not generated by the electromagnetic coils.

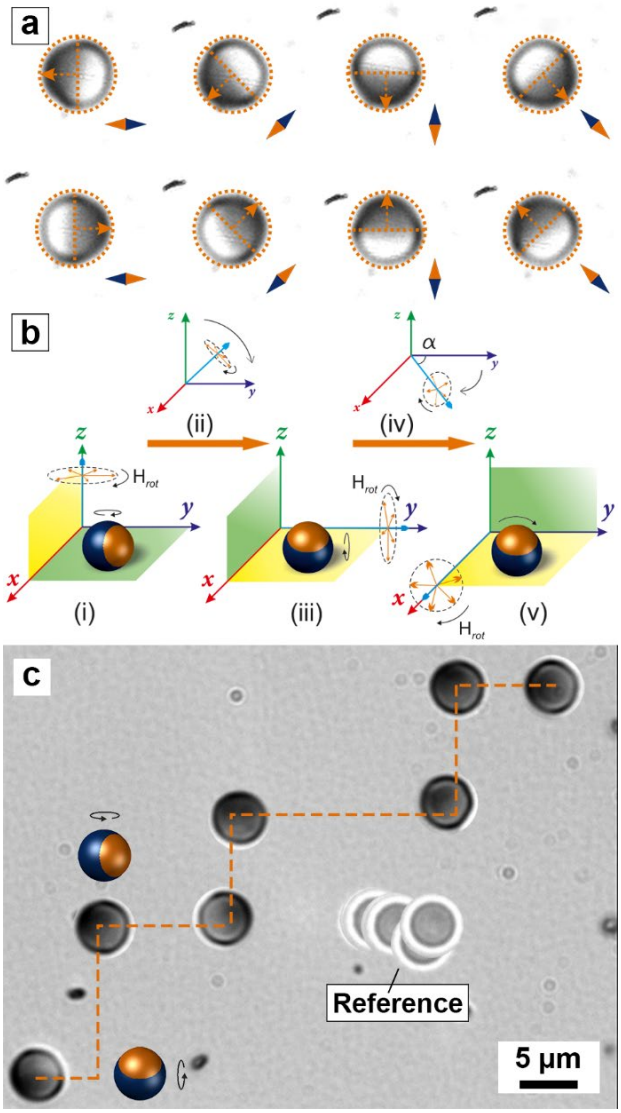

Figure 3 (a) Manipulating the orientation of Janus microsphere by an in-plane rotating magnetic field. Reorientation of the microsphere is demonstrated in Movie S1 (Supporting Information). (b) Schematic illustration of manipulation of the Janus microsphere on a surface. Stage (i) corresponds to the manipulation process in (a). Stage (iii) and (v) indicate that after changing the direction of rotating magnetic field, the rotation of the sphere is converted to translational motion on the surface. (c) Time lapse image of a moving Janus microsphere steered by a rotating magnetic field. A non-coated silica sphere is also given for reference (Movie S2, supporting information).

To propel JMPs on a planar surface, the rotating plane should be changed from parallel to perpendicular to the surface, as is shown in Figure 3(b) (stage ii - stage iii). The friction generated between the microsphere and the surface provides propulsion and generates forward motion. To control

the direction of this motion, the angle α between the y-axis and the normal direction of the rotating magnetic field (the blue arrow, as indicated in stage iv) must be adjusted. For example, if the normal direction of the rotating magnetic field is changed 90 degrees away from the y-axis (i.e. along x-axis), the JMPs will roll sidewards, as illustrated in Figure 3(b) (stage v). As shown in Figure 3(c), the JMPs can be steered along a predefined trajectory. We used a silica particle as a control for magnetic manipulation. As expected, non-magnetic silica particle only exhibited Brownian motion (see Movie S2). The fluid flow generated around the JMP causes a drift in the reference particle's motion only when these particles are in close proximity.

In summary, we report wirelessly controlled ME JMPs consisting of SiO_2 microspheres and ME composite coatings. By introducing magnetostrictive $CoFe_2O_4$ and piezoelectric $BaTiO_3$ layers, electric charges on the ME surface of the JMPs can be wirelessly generated under time-varying magnetic fields. Taking advantage of this phenomenon, electrochemical reactions can be wirelessly induced. Different noble metals such as Ag, Au and Pt were reduced and deposited as metallic nanoparticles. Moreover, the magnetic layer enables these devices to be precisely steered by external magnetic fields. Utilizing a single energy source (magnetic energy) for both navigating the micromachine and triggering its function opens new avenues towards highly integrated devices. Additionally, the proposed ME JMPs offer alternative routes for controlling localized chemical reactions. The implementation of ME building blocks in micro- and nanomachines provides additional functionalities in several applications such as metal recovery, cell electrostimulation or electrically-assisted drug delivery.

Acknowledgements

This work has been financed by the European Research Council Starting Grant "Magnetoelectric Chemonanorobotics for Chemical and Biomedical Applications (ELECTROCHEMBOTS) under the grant no. 336456. X. Z. Chen would like to thank Dr. Yuanxia Zheng at Pennsylvania State University for useful discussion on the PVD sputtering technique, Dr. Houbing Huang at University of Science And Technology Beijing and Dr. Eva Pellicer at Universitat Autònoma de Barcelona for their valuable suggestions. The authors would also like to acknowledge Lydia Zehnder from Institute für Geochemie und Petrologie of ETH for her kind support on XRD measurements, the Scientific Center for Optical and Electron Microscopy (ScopeM) of ETH and the FIRST laboratory for their technical support.

Notes and references

1. B. J. Nelson, I. K. Kaliakatsos and J. J. Abbott, *Annu. Rev. Biomed. Eng.*, 2010, **12**, 55-85.
2. G. Chatzipirpiridis, O. Ergeneman, J. Pokki, F. Ullrich, S. Fusco, J. A. Ortega, K. M. Sivaraman, B. J. Nelson and S. Pane, *Adv. Healthc. Mater.*, 2015, **4**, 209-214.
3. S. Fusco, M. S. Sakar, S. Kennedy, C. Peters, R. Bottani, F. Starsich, A. Mao, G. A. Sotiriou, S. Pane, S. E. Pratsinis, D. Mooney and B. J. Nelson, *Adv. Mater.*, 2014, **26**, 952-957.
4. C. Peters, O. Ergeneman, P. D. W. García, M. Müller, S. Pané, B. J. Nelson and C. Hierold, *Adv. Funct. Mater.*, 2014, **24**, 5269-5276.
5. W. Gao and J. Wang, *ACS Nano*, 2014, **8**, 3170-3180.
6. M. Xuan, X. Lin, J. Shao, L. Dai and Q. He, *ChemPhysChem*, 2015, **16**, 147-151.
7. F. Mushtaq, M. Guerrero, M. S. Sakar, M. Hoop, A. Lindo, J. Sort, X.-Z. Chen, B. J. Nelson, E. Pellicer and S. Pané, *J. Mater. Chem. A*, 2015, DOI:10.1039/C1035TA05825B.
8. J. Li, W. Gao, R. Dong, A. Pei, S. Sattayasamitsathit and J. Wang, *Nat. Commun.*, 2014, **5**, 5026.
9. M. S. Sakar, E. B. Steager, D. H. Kim, M. J. Kim, G. J. Pappas and V. Kumar, *Appl. Phys. Lett.*, 2010, **96**, 043705.
10. L. Zhang, T. Petit, Y. Lu, B. E. Kratochvil, K. E. Peyer, R. Pei, J. Lou and B. J. Nelson, *ACS Nano*, 2010, **4**, 6228-6234.
11. L. Zhang, J. J. Abbott, L. Dong, B. E. Kratochvil, D. Bell and B. J. Nelson, *Appl. Phys. Lett.*, 2009, **94**, 064107.
12. M. A. Zeeshan, R. Grisch, E. Pellicer, K. M. Sivaraman, K. E. Peyer, J. Sort, B. Ozkale, M. S. Sakar, B. J. Nelson and S. Pane, *Small*, 2014, **10**, 1284-1288.
13. B. Jang, E. Gutman, N. Stucki, B. F. Seitz, P. D. Wendel-Garcia, T. Newton, J. Pokki, O. Ergeneman, S. Pane, Y. Or and B. J. Nelson, *Nano Lett.*, 2015, **15**, 4829-4833.
14. D. Ahmed, C. Y. Chan, S. C. Lin, H. S. Muddana, N. Nama, S. J. Benkovic and T. J. Huang, *Lab Chip*, 2013, **13**, 328-331.
15. D. Ahmed, M. Lu, A. Nourhani, P. E. Lammert, Z. Stratton, H. S. Muddana, V. H. Crespi and T. J. Huang, *Sci. Rep.*, 2015, **5**, 9744.
16. R. M. Erb, N. J. Jenness, R. L. Clark and B. B. Yellen, *Adv. Mater.*, 2009, **21**, 4825-4829.
17. E. B. Steager, M. Selman Sakar, C. Magee, M. Kennedy, A. Cowley and V. Kumar, *Int. J. Robot. Res.*, 2013, **32**, 346-359.
18. F. Mou, C. Chen, H. Ma, Y. Yin, Q. Wu and J. Guan, *Angew. Chem. Int. Ed.*, 2013, **52**, 7208-7212.
19. P. H. Colberg, S. Y. Reigh, B. Robertson and R. Kapral, *Acc. Chem. Res.*, 2014, **47**, 3504-3511.
20. S. Sanchez, L. Soler and J. Katuri, *Angew. Chem. Int. Ed.*, 2015, **54**, 1414-1444.
21. A. Servant, F. Qiu, M. Mazza, K. Kostarelos and B. J. Nelson, *Adv. Mater.*, 2015, **27**, 2981-2988.
22. R. S. Rikken, R. J. Nolte, J. C. Maan, J. C. van Hest, D. A. Wilson and P. C. Christianen, *Soft Matter*, 2014, **10**, 1295-1308.
23. T. Xu, J. Yu, X. Yan, H. Choi and L. Zhang, *Micromachines*, 2015, **6**, 1346-1364.
24. J. J. Abbott, K. E. Peyer, M. C. Lagomarsino, L. Zhang, L. Dong, I. K. Kaliakatsos and B. J. Nelson, *Int. J. Robot. Res.*, 2009, **28**, 1434-1447.
25. J.-K. Chen and C.-J. Chang, *Materials*, 2014, **7**, 805-875.
26. H. Meng and G. Li, *Polymer*, 2013, **54**, 2199-2221.
27. R. Ramesh and N. A. Spaldin, *Nat. Mater.*, 2007, **6**, 21-29.
28. J. F. Scott, *J. Mater. Chem.*, 2012, **22**, 4567-4574.
29. M. Xuan, J. Shao, X. Lin, L. Dai and Q. He, *ChemPhysChem*, 2014, **15**, 2255-2260.
30. J. G. S. Moo and M. Pumera, *Chem. Eur. J.*, 2015, **21**, 58-72.
31. G. Zhao and M. Pumera, *Nanoscale*, 2014, **6**, 11177-11180.
32. L. Baraban, D. Makarov, R. Streubel, I. Monch, D. Grimm, S. Sanchez and O. G. Schmidt, *ACS Nano*, 2012, **6**, 3383-3389.
33. W. Gao, X. Feng, A. Pei, Y. Gu, J. Li and J. Wang, *Nanoscale*, 2013, **5**, 4696-4700.
34. L. Baraban, D. Makarov, O. G. Schmidt, G. Cuniberti, P. Leiderer and A. Erbe, *Nanoscale*, 2013, **5**, 1332-1336.
35. L. Baraban, R. Streubel, D. Makarov, L. Han, D. Karnaushenko, O. G. Schmidt and G. Cuniberti, *ACS Nano*, 2013, **7**, 1360-1367.
36. W. Eerenstein, M. Wiora, J. L. Prieto, J. F. Scott and N. D. Mathur, *Nat. Mater.*, 2007, **6**, 348-351.
37. C. Thiele, K. Dörr, O. Bilani, J. Rödel and L. Schultz, *Phys. Rev. B*, 2007, **75**, 054408.
38. J. L. Giocondi and G. S. Rohrer, *Chem. Mater.*, 2001, **13**, 241-242.

39. S. V. Kalinin, D. A. Bonnell, T. Alvarez, X. Lei, Z. Hu, J. H. Ferris, Q. Zhang and S. Dunn, *Nano Lett.*, 2002, **2**, 589-593.
40. C. Rankin, C. H. Chou, D. Conklin and D. A. Bonnell, *ACS Nano*, 2007, **1**, 234-238.
41. A. Haussmann, P. Milde, C. Erler and L. M. Eng, *Nano Lett.*, 2009, **9**, 763-768.
42. Y. Yang, J. Gao, J.-F. Li and D. Viehland, *J. Electrochem. Soc.*, 2011, **158**, K149.
43. R. Guduru, P. Liang, C. Runowicz, M. Nair, V. Atluri and S. Khizroev, *Sci. Rep.*, 2013, **3**, 2953.
44. M. Nair, R. Guduru, P. Liang, J. Hong, V. Sagar and S. Khizroev, *Nat. Commun.*, 2013, **4**, 1707.
45. R. Guduru and S. Khizroev, *Part. Part. Syst. Char.*, 2014, **31**, 605-611.
46. M. B. Starr, J. Shi and X. Wang, *Angew. Chem. Int. Ed.*, 2012, **51**, 5962-5966.
47. X. Guo, *Phys. Chem. Chem. Phys.*, 2014, **16**, 20420-20423.
48. K.-S. Hong, H. Xu, H. Konishi and X. Li, *J. Phys. Chem. C*, 2012, **116**, 13045-13051.
49. M. B. Starr and X. Wang, *Sci. Rep.*, 2013, **3**, 2160.
50. , See online supporting information.
51. R. M. Bozorth, E. F. Tilden and A. J. Williams, *Phys. Rev.*, 1955, **99**, 1788-1798.
52. M. B. Smith, K. Page, T. Siegrist, P. L. Redmond, E. C. Walter, R. Seshadri, L. E. Brus and M. L. Steigerwald, *J. Am. Chem. Soc.*, 2008, **130**, 6955-6963.
53. D. J. R. Appleby, N. K. Ponon, K. S. K. Kwa, S. Ganti, U. Hannemann, P. K. Petrov, N. M. Alford and A. O'Neill, *J. Appl. Phys.*, 2014, **116**, 124105.
54. W. Wang, W. T. Duan, S. Ahmed, T. E. Mallouk and A. Sen, *Nano Today*, 2013, **8**, 531-554.